Research article

Construction of a novel immune response prediction signature to predict the efficacy of immune checkpoint inhibitors in clear cell renal cell carcinoma patients

Jiannan Yao [a,*,1], Ziwei Liang [a,1], Ling Duan [a], Yang G [a], Jian Liu [a,b], Guangyu An [a]

[a] Department of Oncology, Beijing Chao-Yang Hospital, Capital Medical University, Beijing, 100020, China
[b] Medical Research Center, Beijing Chao-Yang Hospital, Capital Medical University, Beijing, 100020, China

ARTICLE INFO

ABSTRACT

Background: Immune checkpoint inhibitor (ICI) treatment has enhanced survival outcomes in clear cell renal cell carcinoma (ccRCC) patients. Nevertheless, the effectiveness of immunotherapy in ccRCC patients is restricted and we intended to develop and characterize an immune response prediction signature (IRPS) to forecast the efficacy of immunotherapy.
Methods: RNA-seq expression profile and clinicopathologic characteristics of 539 kidney cancer and 72 patients with normal specimens, were downloaded from the Cancer Genome Atlas (TCGA) database, while the Gene Expression Omnibus (GEO) database was used as the validation set, which included 24 ccRCC samples. Utilization of the TCGA data and immune genes databases (ImmPort and the InnateDB), we explored through Weighted Gene Co-expression Network Analysis (WGCNA), along with Least Absolute Shrinkage and Selection Operator method (LASSO), and constructed an IRPS for kidney cancer patients. GSEA and CIBERSORT were performed to declare the molecular and immunologic mechanism underlying the predictive value of IRPS. The Human Protein Atlas (HPA) was deployed to verify the protein expressions of IRPS genes. Tumor immune dysfunction and exclusion (TIDE) score and immunophenoscore (IPS) were computed to determine the risk of immune escape and value the discrimination of IRPS. A ccRCC cohort with anti-PD-1 therapy was obtained as an external validation data set to verify the predictive value of IRPS.
Results: We constructed a 10 gene signature related to the prognosis and immune response of ccRCC patients. Considering the IRPS risk score, patients were split into high and low risk groups. Patients with high risk in the TCGA cohort tended towards advanced tumor stage and grade with poor prognosis (p < 0.001), which was validated in GEO database (p = 0.004). High-risk group tumors were related with lower PD-L1 expression, higher TMB, higher MSIsensor score, lower IPS, higher TIDE score, and enriched Treg cells, which might be the potential mechanism of immune dysfunction and exclusion. Patients in the IRPS low risk group had better PFS (HR:0.73; 95% CI: 0.54–1.0; P = 0.047).
Conclusion: A novel biomarker of IRPS was constructed to predict the benefit of immunotherapy, which might lead to more individualized prognoses and tailored therapy for kidney cancer patients.

* Corresponding author.
  E-mail address: yaojiannan@ccmu.edu.cn (J. Yao).
[1] These authors have contributed equally to this work and share first authorship.

1. Introduction

Renal cell carcinoma (RCC) is the second commonly diagnosed urologic neoplasm worldwide, with about 79,000 new cases and 13,920 deaths in 2022 [1]. Among all subtypes of RCC, approximately 70%–85% of cases are categorized as clear cell renal cell carcinoma (ccRCC) [2]. Conventional chemotherapy and radiotherapy of ccRCC are invalid, and interleukin 2 (IL-2) and interferon alpha (IFN-a) are diffusely applied despite limited effect [3]. Although the targeted therapy has improved immensely, metastatic ccRCC has a dismal 12% 5-year survival rate [4]. Fortunately, the development of immune checkpoint inhibitor (ICI) treatment is profoundly changing the treatment situation for many cancers. FDA-approved ICIs, including nivolumab and pembrolizumab, have become routine treatment for ccRCC, with numerous clinical trials demonstrating their profound benefits in improving patient overall survival [5–7]. Nevertheless, due to immune dysfunction and exclusion, not all ccRCC patients demonstrate sensitivity to this important treatment modality. Recent studies demonstrate that WDR5, a histone H3 lysine 4 (H3K4) presenter, is upregulated in a variety of cancers and has a positive correlation with PD-L1 expression. It plays a vital role in proliferation, self-renewal, and cisplatin chemoresistance in bladder cancer [8]. Moreover, WDR5 also plays an important role in lymphatic metastasis of bladder cancer through the HSF1-PRMT5-WDR5 axis [9]. Therefore, targeting WDR5 may be a novel therapeutic concept to concurrently inhibit proliferation and PD-L1 expression in bladder cancer. In addition to this, HHLA2 expression is much higher than that of PD-L1 in ccRCC tissues, and is significantly associated with worse outcome. Moreover, patients with HHLA2/PD-L1 co-expression associated with adverse outcomes. HHLA2 could decrease the proliferation and the function of CD8$^+$ and CD4$^+$ TILs and inhibit the production of cytokines. In this way, anti-HHLA2 may have potential as a novel immunotherapy [10]. However, despite the discovery of numerous new treatments and immune mechanisms, the efficacy of immunotherapy in each individual ccRCC patient is still unknown. Therefore, it is essential to determine new predictive factors for ICI efficacy. Currently, various biomarkers are reported to have predictive value for ICI efficacy. Specifically, high PD-L1 expression, identified with high tumor mutational burden (TMB), or with microsatellite instability (MSI-H) state, or with mismatch repair deficient (dMMR), always forecast benefits from ICI therapy [11–13]. However, none of these markers have been sufficiently verified to precisely predict ICI reaction [14]. ccRCC has unique features in terms of the immune microenvironment. Previously defined biomarkers have failed to split ccRCC patients into high or low immune response groups, while some studies even show that ccRCC patients with high TMB presented to determine a lower reaction rate to immunotherapy [15,16]. Consequently, in order to resolve the aforementioned problem, there is an urgent need to develop a reliable biomarker in ccRCC patients to predict the survival outcomes and the immune response.

In the present project, we established a novel ten-gene signature linked with the immune microenvironment to forecast immunotherapy effectiveness and survival outcomes of ccRCC patients, using the publicly available RNA-seq expression data from The Cancer Genome Atlas (TCGA) and NCBI GEO. Tumor immune dysfunction and exclusion (TIDE) score was employed in our research, in order to represent the risk of immune escape and forecast the effectiveness of ICIs treatment in ccRCC. Furthermore, we systematically interrogated the potential molecular and immunologic mechanisms underlying IRPS's prognostic ability. These findings should be useful to clinicians in providing more individualized prognoses and tailored therapy.

2. Materials and methods

2.1. Research project and data acquisition

The entire candidate generation design is presented as a flow plot in Fig. 1.

The publicly available TCGA database was applied to obtain the RNA-seq (HTSeq-FPKM) expression profiles (https://portal.gdc.cancer.gov/). Ultimately, 539 ccRCC samples were retrieved, while 72 specimens in normal tissue were also enrolled. A GTF file from GENCODE (https://www.gencodegenes.org/) was obtained, in order to annotate genes. The corresponding clinicopathological information of 542 cancer samples were acquired from the TCGA-KIRC GDC dataset maintained by the UCSC Cancer Genmoe Browser (https://xenabrowser.net/). We acquired gene names from the ImmPort (https://www.immport.org/) and InnateDB (https://www.innateDBdb.com/) databases, which contained 6196 genes related to immunology. Meanwhile, GSE22541 dataset was obtained as the external validation set, consisting of acquirable RNA-seq expression information and patient outcomes for 24 ccRCC tumor specimens, from the NCBI Gene Expression Omnibus (NCBI GEO) (https://www.ncbi.nlm.nih.gov/geo/).

2.2. Exploration of immune-related differentially expressed genes (IRDEGs)

To screen out the differentially expressed genes (DEGs) between ccRCC samples and regular tissue samples, we utilized the "limma" package in R. We regarded the median as the gene expression value if different probes were associated with the same gene. The Benjamin-Hochberg correction was adopted to adjust P-value, and a False Discovery Rate (FDR) < 0.05, with |log-fold change (log-FC)| >1 was selected as the thresholds for DEG screening. After that, IRDEGs were defined as the intersection of DEGs and the cluster of genes in immune-related genes list.

2.3. Function analysis of IRDEGs

Gene Ontology (GO) was enrolled to explore the potential function by "ClusterProfiler" R package. Meanwhile, the Kyoto Encyclopedia of Genes and Genomes (KEGG) analyses was also performed for the purpose of exploring the functional signaling pathways of
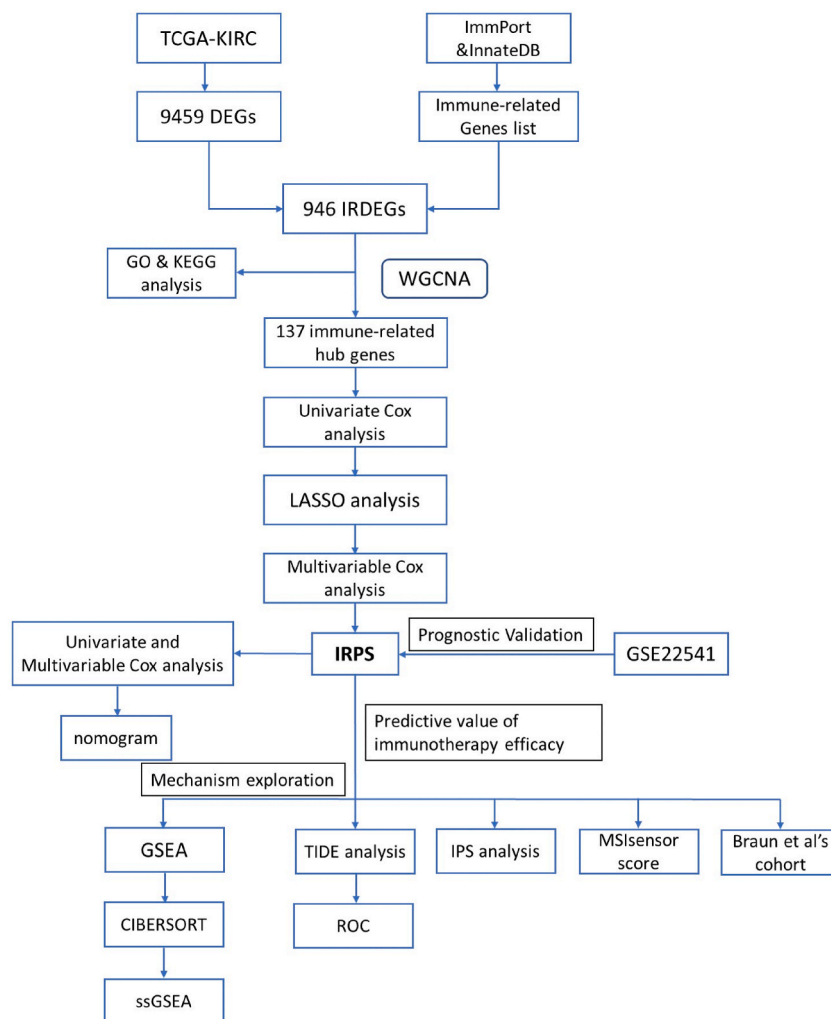
Fig. 1. Flow diagram of the whole project design.

IRDEGs. The significant results of GO and KEGG were painted with the "GOplot" R package.

2.4. Weighted gene co-expression network analysis (WGCNA)

To acquire hub genes related with immune function, "WGCNA" R package was envolved in this research [17]. First, sample clustering analysis was constructed based upon the association coefficient between two genes using Pearson's test. Second, we set a soft threshold to fit the scale-free network law, based on a scale-free R2 of 0.9, for the juxtaposition matrix. Accordingly, a topological overlap matrix with topological overlap measure (TOM) was carried out. 1-TOM was utilized to group genes with similar patterns of expression, and a dynamic hybrid tree cutting algorithm was further used to identify the modules. The IRDEG expression in tumor tissues and normal tissues were considered as clinical traits. The genes of significantly related modules were selected for subsequent analysis.

2.5. Construction of the immune response prediction signature (IRPS)

We used Univariate Cox proportional hazards regression analysis for further identification of the independent and significantly predictive genes according to the overall survival (OS). The "glmnet" R package with the use of applying the Least Absolute Shrinkage and Selection Operator method (LASSO) was conducted, for screening of the best matched predictive signatures for constructing a multi-gene prognostic signature. Next, the candidates were used in multivariate Cox proportional hazards regression analysis to develop IRPS. Subsequently, the risk model was established with a risk score defined as: risk score = expression of gene1 × Coef1 + expression of gene2 × Coef2 + …… + expression of gene n × Coef n. Next, according to the risk score, patients were divided into high risk and low risk subgroups. The optimal cut-off point of IRPS risk score was determined through "survminer" R package. Furthermore,

for verifying the protein expression of IRPS genes, the Human Protein Altas (HPA) database (https://www.proteinatlas.org/) was further used.

2.6. Survival analysis and confirmation of the independent predictive value of IRPS

To investigate IRPS for predictive ability, Kaplan–Meier survival analysis was propelled to present the survival curves, meanwhile, the log-rank tests were deployed to compare the differences in both the TCGA and GEO cohorts. Existing clinicopathological information from databases such as age, gender, tumor laterality, tumor grade, tumor stage, T stage, N stage and M stage were all included with the risk score, while univariate and multivariate Cox proportional hazards regression analysis was deployed to validate the independent predictive ability of IRPS. The outcomes were visualized with forest plots.

2.7. Analysis of the molecular and immunologic mechanism

Determination of the potential biological signaling pathways between the two IRPS risk groups was conducted by "clusterProfiler" and the "org.Hs.eg.db" R package through Gene set enrichment analysis (GSEA). The immunological signature gene set (c2.cp.kegg. v7.4.symbols.gmt) and the reference set of GSEA was selected. The different gene mutations among IRPS risk groups were researched and painted into waterfall plots through "Maftools" package in R. To identify the differences in immune characteristics between the two risk groups, CIBERSORT was applied to evaluate the proportion of 22 subtypes of immune-related cells in the two groups. Moreover, single sample GSEA (ssGSEA) was performed with the "GSVA" R package for the purpose of analyzing immune and molecular function.

2.8. Predictive role of IRPS for immunotherapy efficacy

Tumor Immune Dysfunction and Exclusion (TIDE) score (HTTP://tide.dfci.harvard.edu/) was used to identify the prognostic value of the IRPS in the effectiveness of immunotherapy. We also validated our model and compared with other immune-related gene signatures [18] with the "survivalROC" R package and computed the area under the curve (AUC) of the receiver operator characteristic (ROC) curve. In addition, the MSI status, measured by MSIsensor score, was considered in this project as an ICI response biomarker. Furthermore, the immunophenoscore (IPS) of ccRCC patients were obtained from the Cancer Immunome Atlas (TCIA) database, as an assessment indicator for tumor immunogenicity to predict the response to immunotherapy. To evaluate IRPS-associated outcomes in a realistic scenario, we obtained clinical and molecular data from a ccRCC cohort treated with anti-PD-1 therapy [19]. Braun et al.'s ccRCC cohort included available RNA-seq expression data and clinical data of 309 patients with ccRCC, who underwent anti-PD-1 therapy.

2.9. Statistical analysis

Comparison of continuous variables between risk subgroups was performed through the independent t-test. Categorical characteristics were examined with the utilization of the chi-square test and Fisher test. Differences in PD-L1 expression as well as TMB and TIDE score between risk subgroups were examined by the Wilcoxon test. The survival analyses were proceeded and calculated through the Kaplan–Meier method and at the same time, difference between curves were estimated with the log-rank test. We considered a two-sided P-value < 0.05 to be remarkable difference.

3. Results

3.1. Identification and enrichment analysis of IRDEGs

To acquire the DEGs, 611 specimens of ccRCC were retrieved in total from the TCGA database, including RNA-seq expression of 539 samples in ccRCC and 72 samples in normal tissue. Using the filtering criteria of FDR < 0.05 and |log₂(FC)| > 1, 9459 DEGs in ccRCC were recognized, among these genes, 7191 genes were implied to have up-regulation,while other 2268 down-regulated genes were also acquired (Fig. S1A). Additionally, 2660 genes related to immune function were downloaded from the webset of ImmPort and InnateDB. After intersecting the DEGs and immune-related genes, 946 immune-related differentially expressed genes (IRDEGs) were performed (Fig. S1B). The functional enrichment analysis was performed using GO and KEGG databases to explore the potential biological function of IRDEGs (Fig. 2). In the GO analysis chord plot, the top 8 terms related to the IRDEGs were leukocyte mediated immunity, adaptive immune response based on somatic recombination of immune receptors built from immunoglobulin superfamily domains, lymphocyte mediated immunity, positive regulation of cell activation, positive regulation of leukocyte activation, production of molecular mediator of immune response, positive regulation of lymphocyte activation, and B cell mediated immunity (Fig. 2A). In the KEGG pathway analysis, "Cytokine cytokine receptor interaction" was implied to be the most notable immune-related enriched pathway (Fig. 2B).

3.2. Determination of immune-related hub genes using WGCNA

We carried out Weighted Gene Correlation Network Analysis (WGCNA) of the 946 IRDEGs to acquire immune-related hub genes.
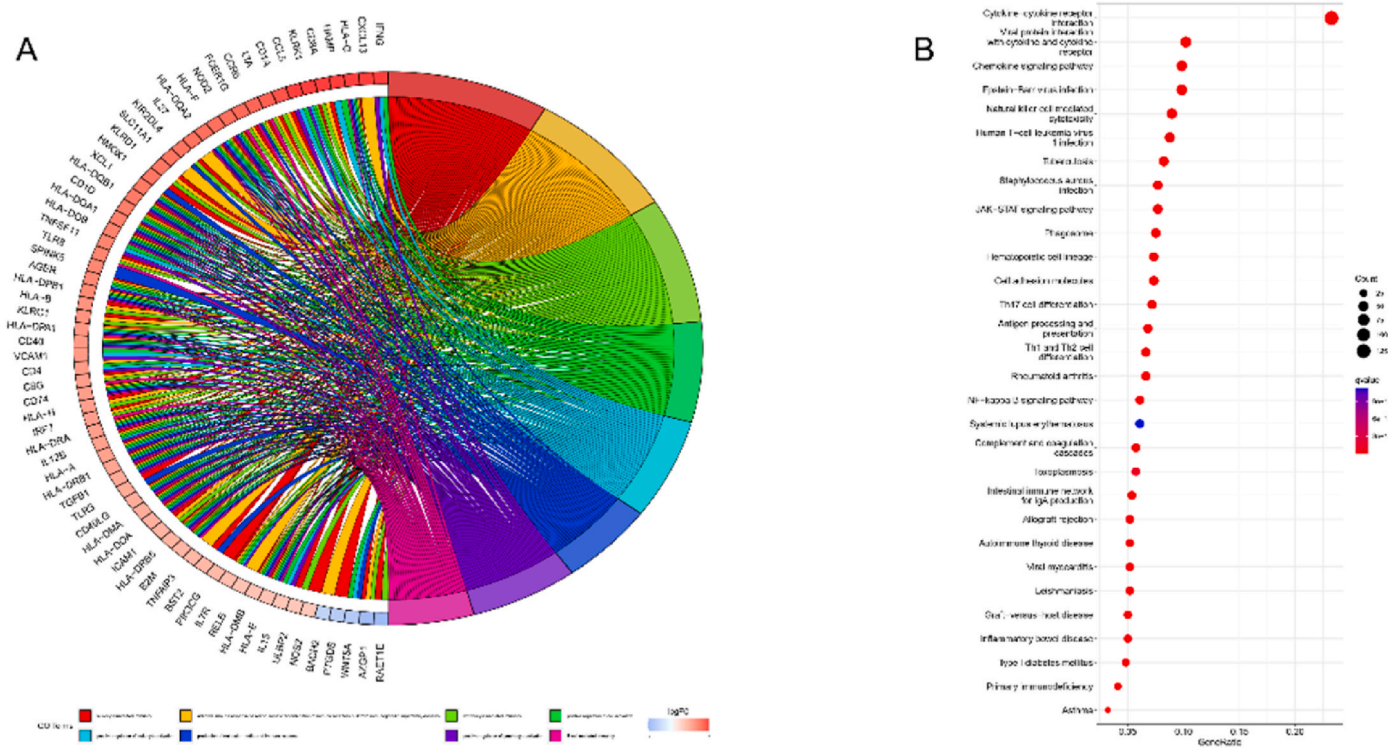
Fig. 2. Functional enrichment of IRDEGs. A. The top 8 terms of GO enrichment analysis of IRDEGs B. The top 30 KEGG enrichment analysis of IRDEGs, "Cytokine cytokine receptor interaction" was the most notable immune-related enriched pathway.
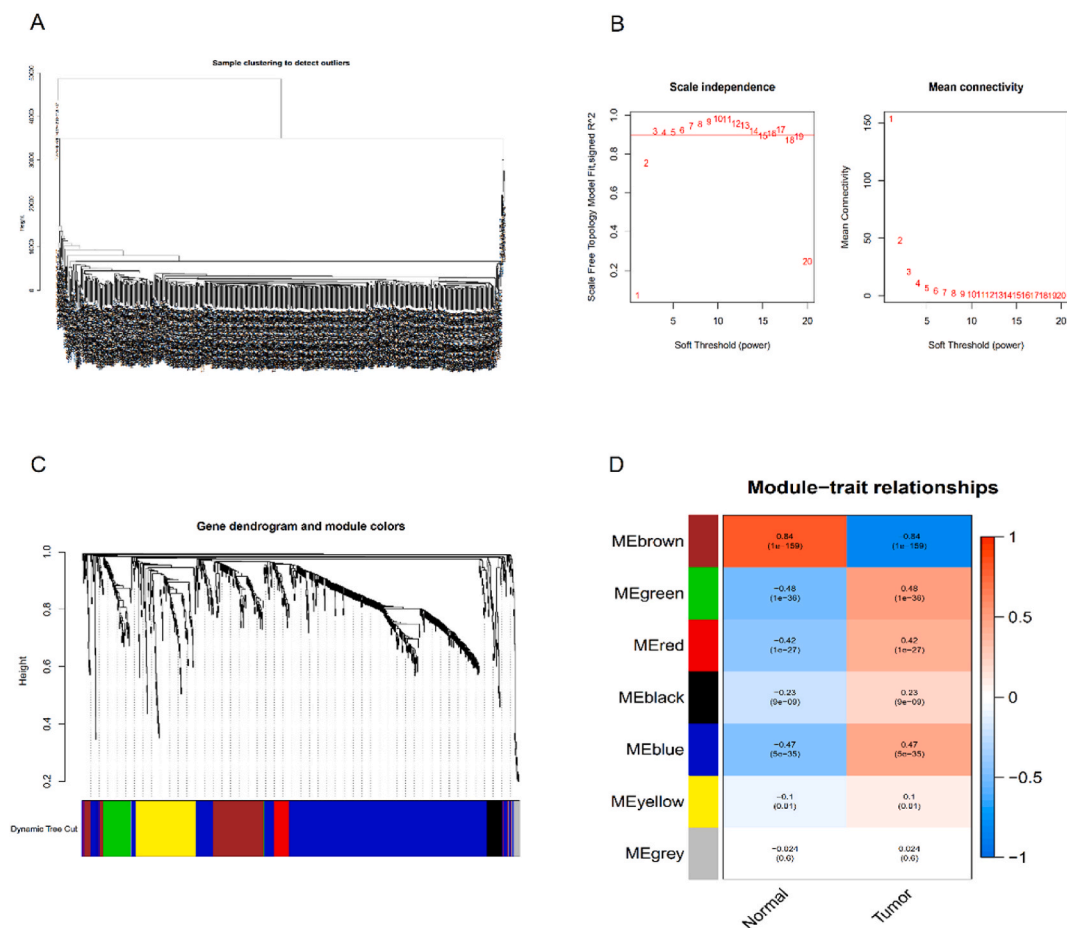
Fig. 3. Weighted gene co-expression network analysis (WGCNA) of the IRDEGs. A. The samples clustering tree to detect outliers, height greater than 20,000 has been removed. B. Determination of the optimal soft-thresholding powers. Pick the soft-thresholding power of 3 to satisfy the scale-free network law based on a scale-free R2 = 0.9. C. Gene dendrogram and module colors. Each branch in the dendrogram represents genes, and genes clustered into the same module will have the same module color. D. The heatmap of the correlation between tumor trait and gene module.

First, we removed some stray samples, which had a height in the hierarchical clustering tree of greater than 20,000 (Fig. 3A). The correlation coefficient was greater than 0.9, and we picked the optimal soft-thresholding power of "3" to fulfill the scale-free network rule (Fig. 3B). Genes with similar expression patterns clustered into the same module and retained the module color (Fig. 3C). Six modules were identified using the dynamic pruning method, including brown, green, red, black, blue and yellow modules, while the gray module included genes lacking any expression relationship with other genes. Among them, the most significant correlation with tumor traits was the brown module, which contained 137 immune-related hub genes (Fig. 3D). Therefore, the module with brown color was eventually chosen for the further establishment of IRPS.

3.3. Construction of the immune response prediction signature (IRPS)

We selected the 137 immune-related hub genes from the brown module, and based on these genes, 57 candidates were obtained by Univariate Cox proportional hazards regression analysis as independently prognostic of OS (Table S1). Among them, 19 of these genes were OS risk factors, while the remaining 35 genes were protective factors (Fig. 4A). Next, we used LASSO regression analysis to exclude overfitting genes and ultimately screened out 21 optimal genes with prognostic value for constructing of a multi-gene prognostic signature (Fig. 4B and C). These 21 genes were further incorporated in multivariate Cox proportional hazards regression analysis. The Akaike information criterion (AIC) was considered in order to construct the best-fit prognostic model, and finally a 10 immune-related genes signature was selected as the IRPS (Fig. 4D). The 10 genes were TMSB4Y, NDRG1, SEMA3G, SEMA6D, BMP1, TSLP, MCHR1, SHC1, PRKX and TRIM55. Among these genes, the expression of BMP1, TSLP, MCHR1 and SHC1 were associated with worse outcomes, while TMSB4Y, NDRG1, SEMA3G, SEMA6D and PRKX were down-regulated and positively associated with patient survival (Table S2).

The protein expression of IRPS genes in regular samples and cancer tissues were explored utilizing the HPA database. We involved all normal kidney samples (three normal kidney samples) from the HPA database as the control group, and chose three typical ccRCC
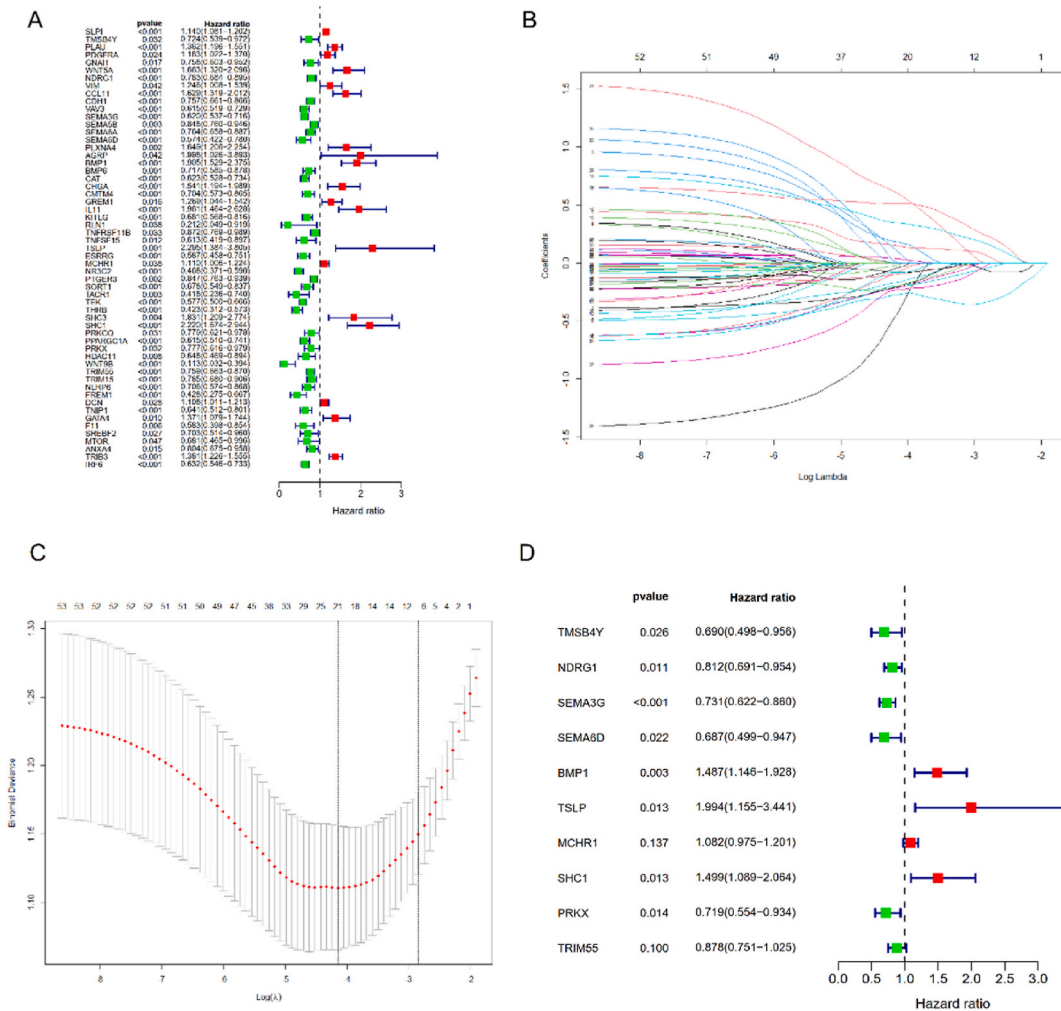
Fig. 4. Construction of an immune response prediction signature (IRPS). (A) Univariate Cox regression analysis for 54 immune-related hub genes demonstrates that 19 genes are OS risk factors, while the remaining 35 genes are protective factors. (B, C) the Least Absolute Shrinkage and Selection Operator (LASSO) regression analysis for the 54 immune-related hub genes. (D) Multivariate Cox regression analysis for immune-related hub genes performs that 4 genes are OS risk factors, other 6 genes are protective factors.

IHC samples as the experimental group. ImageJ was used to calculate the proportion of positive staining, and the results were analyzed using the Mann-Whitney U test to determine significance. We found the protein expression of SHC1 and NDRG1 in normal kidney tissue was lower than that in tumor tissue (P < 0.001) (Fig. 5A and B), while the protein expression of PRKX was not significantly different between normal kidney tissue and tumor tissue (P = 0.916) (Fig. 5C).

Next, we constructed an IRPS risk score formula with the gene expression and regression coefficient: risk score = $(-0.371 \times$ expression of TMSB4Y) + $(-0.208 \times$ expression of NDRG1) + $(-0.313 \times$ expression of SEMA3G) + $(-0.375 \times$ expression of SEMA6D) + $(0.397 \times$ expression of BMP1) + $(0.690 \times$ expression of TSLP) + $(0.079 \times$ expression of MCHR1) + $(0.405 \times$ expression of SHC1) + $(-0.330 \times$ expression of PRKX) + $(-0.131 \times$ expression of TRIM55). After that, utilizing the formula, each ccRCC patient was marked with their IRPS risk score. Based upon the optimal cut-off points of IRPS risk score, we distributed patients in the TCGA cohort and developed two risk subgroups. Patients with higher IRPS risk score were divided into the high-risk subgroup, while patients with lower IRPS risk score were in the low-risk subgroup.

3.4. Survival analysis and validation of the independent prognostic value of IRPS

IRPS had prognostic value and the best cut-off point of risk score successfully had the ability to identify two risk subgroups. As shown in Fig. 6, the KM survival curve presented that low-risk subgroups owned better survival outcomes than high-risk group (p < 0.001, Fig. 6A) in TCGA cohort. An external validated data of GEO cohort (GSE22541) was involved to validate the predictive ability of IRPS (p = 0.004, Fig. 6B) and it also indicated better OS in IRPS low-risk group, consistent with the result in TCGA cohort.

974 samples of ccRCC with clinicopathologic information were downloaded from UCSC Xena, including 542 primary tumor
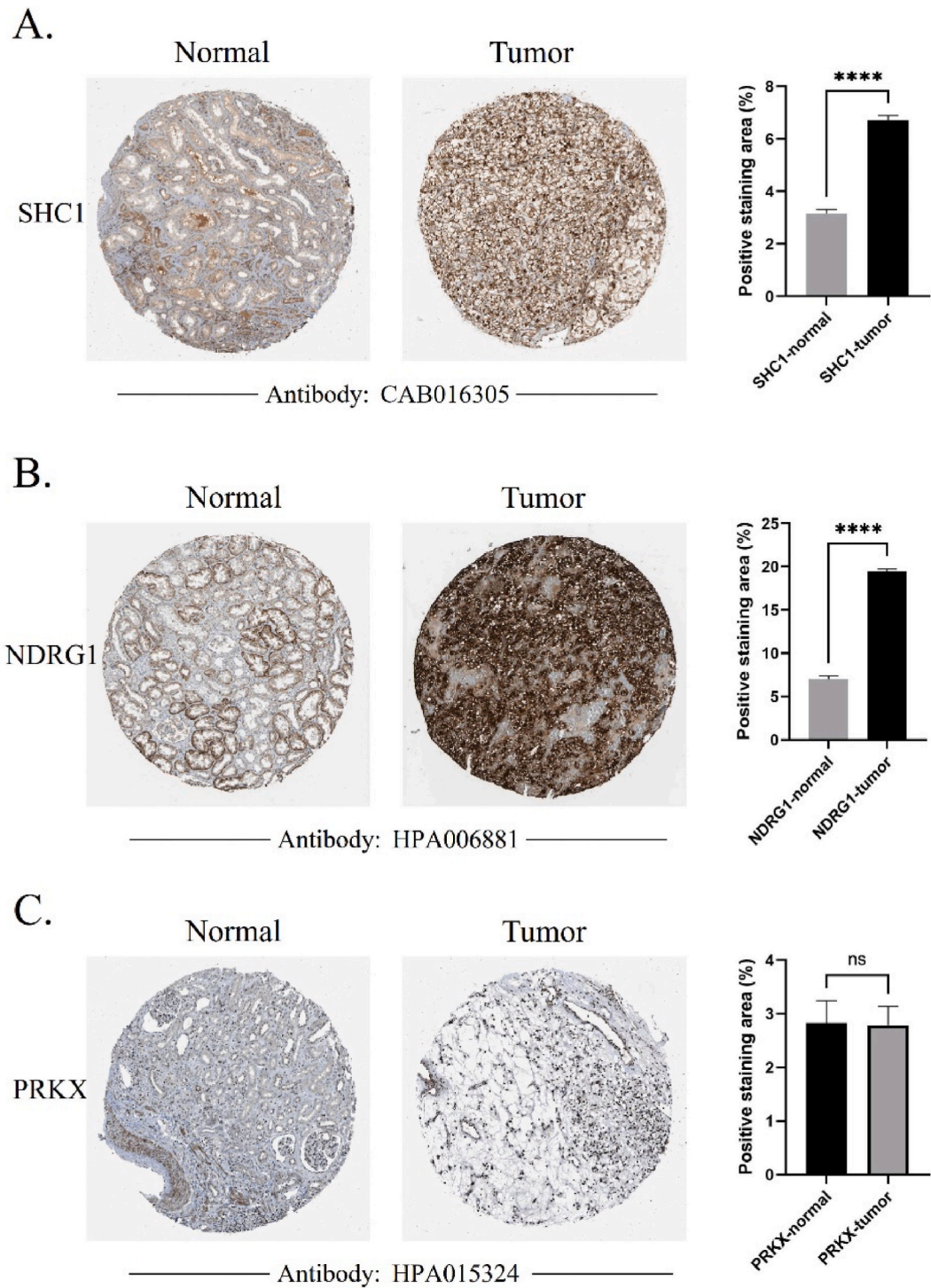
Fig. 5. The protein expression of SHC1, NDRG1 and PRKX in normal kidney tissue and tumor tissue. (A) The protein expression of SHC1 in normal kidney tissue was lower than that in tumor tissue (P < 0.001). (B) The protein expression of NDRG1 in normal kidney tissue was lower than that in tumor tissue (P < 0.001). (C) The protein expression of PRKX was not significantly different between normal kidney tissue and tumor tissue (P = 0.916).
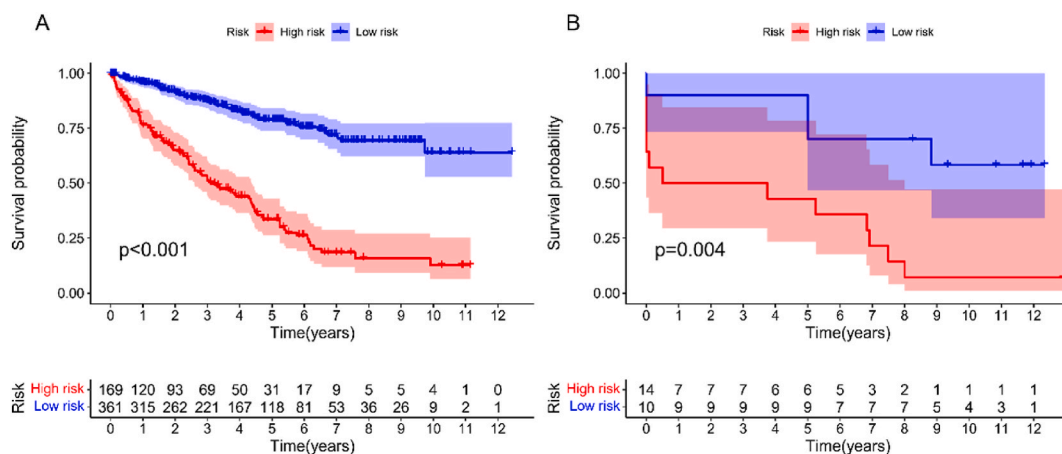
Fig. 6. Prognostic analysis of high risk and low risk cases in TCGA cohort and GEO cohort. (A) Kaplan-Meier survival analysis of the IRPS subgroups in the TCGA cohort performs that the low-risk subgroups own better survival outcomes than high-risk group (p < 0.001). (B) Kaplan-Meier survival analysis of the IRPS subgroups in the GEO cohort indicates that low-risk subgroups own better survival outcomes than high-risk group (p = 0.004).

samples. We analyzed several clinicopathologic features including age, sex, tumor laterality, tumor grade, tumor stage, T stage, N stage and M stage. The clinical characteristics and IRPS subgroups in TCGA cohort are demonstrated in Table 1.

We detected that IRPS risk score appeared to have relationship with all characteristics except gender. The majority of ccRCCs were male (344, 64.9%), and the average age was 60.6 years. Approximately half of patients were diagnosed at an early stage without distant metastasis and grade II-III disease. There were a total of 169 IRPS high-risk patients and meanwhile, with other 361 IRPS low-risk patients. Patients in the IRPS high-risk group (62.4 ± 12.3 years old) were older on average compared to the low-risk group (59.7 ± 11.9 years old) (P = 0.015). The high-risk group was probably presented to be cooperated with left laterality, grade III-IV, and stage III-IV disease. High-risk group patients had greater probability of suffering distant metastasis compared with the low-risk group. The distribution of the clinical factors between the IRPS risk-groups is shown in the heat map and table (Fig. 7A and B).

The IRPS high-risk group tended to present with an advanced stage (stage III-IV, 62.7%) and advanced grade (grade III-IV, 77.5%), which was associated with worse survival outcomes. Moreover, IRPS was an isolated biomarker for OS (Table 2).

Univariate Cox proportional hazards regression analysis performed that age, grade, stage, T, N, M and IRPS risk score seemed to be significantly related to OS (P < 0.05, Fig. 8 A). Furthermore, multivariate Cox proportional hazards regression analysis demonstrated that age and IRPS risk score were independent factors and had prominent association with OS (P < 0.001, Fig. 8B), which confirmed that even after ignoring other interferential factors, IRPS risk score was still an independent signature of prognosis.

Finally, we constructed a nomogram for visualization, which could be applied as a mensurable tool for forecasting prognosis of ccRCC patients (Fig. 9A). The C-index of the nomogram was 0.765. The 1-year, 2-year, and 3-year calibration curves were all close to the 45° diagonal line, which illustrates that the nomogram has a high accuracy (Fig. 9B).

3.5. Analysis of the molecular and immunologic mechanism of IRPS

We further researched the possible molecular mechanism and immunologic theory underlying the predictive and prognostic role of IRPS. The immunological signature gene set (c2.cp.kegg.v7.4.symbols.gmt) was proceed to perform GSEA of possible biological signaling pathways. As shown in Fig. 10A, the top 5 immune functions of IRPS high-risk subgroup were complement and coagulation cascades, cytokine-cytokine receptor interaction, ECM receptor interaction, NOD link receptor signaling pathway and type I diabetes mellitus. While propanoate metabolism, renin angiotensin system, tight junction, valine leucine and isoleucine degradation, vibrio cholerae infection were enriched in the IRPS low-risk group (Fig. 10B). The identification of gene mutation rates between two subgroups was illustrated through a waterfall plot (Fig. 10C). The immunological signature gene set (c7.immunesigdb.v2022.1.Hs.symbols.gmt) was downloaded from the GSEA molecular signatures database to perform GSEA analysis. The top 5 gene sets of immune-related cells were significantly different within the IRPS risk subgroups. The enrichment of B cells and natural T reg cells were observed in the IRPS high-risk group, while CD4 T cells, CD4 follicular helper T cells, NK cells and CD8 T cells were enriched in IRPS low-risk group (Fig. 10C and D).

The waterfall plot presented the significantly different mutated genes within the high risk and low risk IRPS subgroups (Fig. 10 E and F). VHL, PBRM1 and TTN gene mutations were the most frequent in all ccRCCs. The mutation of the HMCN1 and SPEN was higher in the high-risk subgroup. The Immune characteristics of two IRPS subgroups was assessed by CIBERSORT to visualize the proportion of immune cells (Fig. 11A and B). In the IRPS high-risk subgroup, Plasma cells, T cells CD4 memory activated, T cells follicular helper, T cells regulatory (Tregs) and Macrophages M0 were more abundant. Meanwhile, T cells CD4 memory resting, Monocytes, Macrophages M2, Dendritic cells resting and Mast cells resting were more abundant in IRPS low-risk group. Furthermore, ssGSEA as a method of exploring immune and molecular function was applied in this project, and meanwhile, comparison of the score between the risk groups was performed (Fig. 11C). The high-risk group contained high scores for aDCs, APC co-stimulation, CCR, CD8+T cells, check point,

Table 1
Clinical characteristics and IRPS subgroups in TCGA cohort.

| Variables	TCGA cohort	IRPS risk score		P value
	n (%)	Low	High	
Age (mean ± SD)	60.6 ± 12.1	59.7 ± 11.9	62.4 ± 12.3	0.015
Gender				
Male	344 (64.9)	238 (65.9)	106 (62.7)	0.471
Female	186 (35.1)	123 (34.1)	63 (37.3)	
Laterality				
Left	249 (47.0)	159 (44.0)	90 (53.3)	0.043
Right	280 (52.8)	202 (56.0)	78 (46.2)	
Grade				
G1	14 (2.6)	14 (3.9)	0	<0.001
G2	227 (42.8)	191 (52.9)	36 (21.3)	
G3	206 (38.9)	130 (36.0)	76 (45.0)	
G4	75 (14.2)	20 (5.5)	55 (32.5)	
GX	5 (0.9)	4 (1.1)	1 (0.6)	
unknown	3 (0.6)	2 (0.6)	1 (0.6)	
Stage				
I	265 (50.0)	219 (60.7)	46 (27.2)	<0.001
II	57 (10.8)	41 (11.4)	16 (9.5)	
III	123 (23.2)	60 (16.6)	63 (37.3)	
IV	82 (15.5)	39 (10.8)	43 (25.4)	
Unknown	3 (0.5)	2 (0.5)	1 (0.6)	
T				
T1	271 (51.1)	222 (61.5)	49 (29.0)	<0.001
T2	69 (13.2)	48 (13.3)	21 (12.4)	
T3	179 (33.7)	89 (24.7)	90 (53.3)	
T4	11 (2.0)	2 (0.5)	9 (5.3)	
N				
N0	239 (45.1)	159 (44.1)	80 (47.3)	<0.001
N1	16 (3.0)	4 (1.1)	12 (7.1)	
NX	275 (51.9)	198 (54.8)	77 (45.6)	
M				
M0	420 (79.2)	299 (82.8)	121 (71.6)	<0.001
M1	78 (14.7)	37 (10.2)	41 (24.3)	
MX	30 (5.7)	23 (6.4)	7 (4.1)	
Unknown	2 (0.4)	2 (0.6)	0	
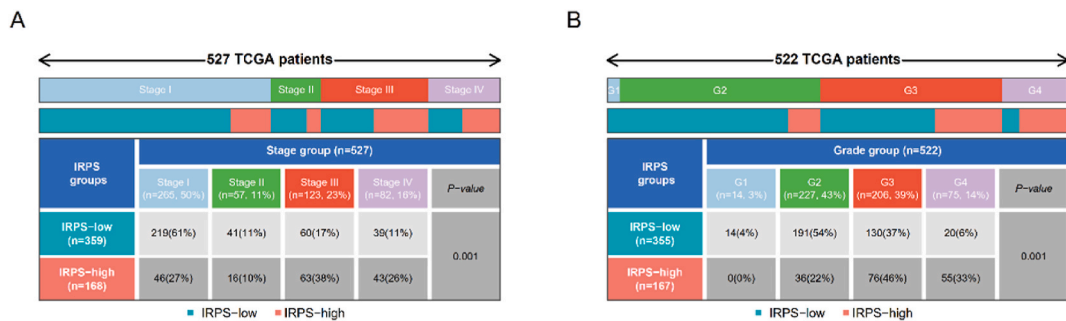
Fig. 7. Heat map and table showing the distribution of the clinical information between the IRPS subgroups. (A) High-risk group patients have greater probability of diagnosing stage III-IV. (B) High-risk group patients have greater probability of diagnosing grade III-IV.

cytolytic activity, inflammation promoting, Macrophages, Parainflammation, T cell co-inhibition, T cell co-stimulation, T helper cells, Tfh, Th1 cells, Th2 cells, TIL and Treg. The low-risk group had high scores for iDCs, Mast cells and type II IFN response.

3.6. Predictive role of IRPS for immunotherapy efficacy

The relationship between IRPS and immune response was further explored to identify the predictive role of IRPS for the efficacy of immunotherapy. PD-L1 expression as well as Tumor Mutation Burden (TMB) are considered predictive factors for the immune response in patients with malignant tumor. We confirmed the relationship between IRPS risk score and the expression of PD-L1 and TMB. The IRPS low-risk subgroup had higher PD-L1 expression (P < 0.001, Fig. 12A) and lower TMB (P = 0.0013, Fig. 12C). IRPS risk score negatively correlated with PD-L1 expression (R = −0.2, P < 0.001, Fig. 12B) and positively associated with TMB (R = 0.24, P < 0.001, Fig. 12D), which confirmed that the high-risk group may potentially fail to respond to immunotherapy.

Table 2

Univariate and multivariate Cox regression analyses of the TCGA cohort.

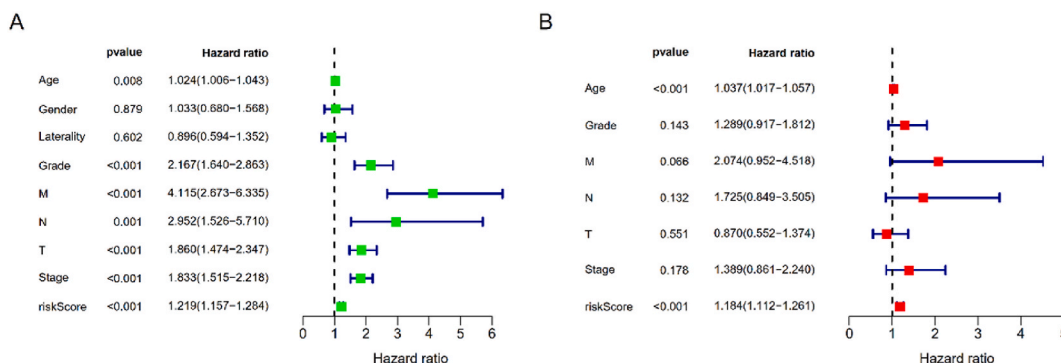|	Univariate analysis		Multivariate analysis	
Variables	HR (95%CI)	P value	HR (95%CI)	P value
Age	1.02 (1.01–1.04)	0.008	1.04 (1.02–1.06)	<0.001
Gender	1.03 (0.68–1.57)	0.879		
Laterality	0.90 (0.59–1.35)	0.602		
Grade	2.17 (1.64–2.86)	<0.001	1.29 (0.92–1.81)	0.143
T	1.86 (1.51–2.22)	<0.001	0.87 (0.55–1.37)	0.551
N	2.95 (1.53–5.71)	0.001	1.72 (0.85–3.51)	0.132
M	4.11 (2.67–6.34)	<0.001	2.07 (0.95–4.52)	0.066
Stage	1.83 (1.51–2.22)	<0.001	1.39 (0.86–2.24)	0.178
riskScore	1.22 (1.16–1.28)	<0.001	1.18 (1.11–1.26)	<0.001

Fig. 8. Univariate and multivariate Cox regression analysis forest plot of TCGA cohort reveals that the risk score is an independent prognostic factor. (A) univariate Cox regression analysis forest plot of TCGA cohort performs that age, grade, stage, T, N, M and IRPS risk score seem to be significantly related to OS(P < 0.05). (B) multivariate Cox regression analysis forest plot of TCGA cohort performs that IRPS risk score is an independent signature of prognosis (P < 0.001).

MSI status as an ICI response biomarker was also considered in our project. Patients with MSI-high status are reported to have better prognosis and response to ICI therapy [14,20]. MSIsensor score, a quantitative measure of MSI [21], was calculated within IRPS risk subgroups. In our project, patients in the IRPS low-risk group had a higher MSIsensor score (P = 0.012, Fig. 13), which further illustrated that the IRPS low risk group might benefit from ICI therapy.

Additionally, TIDE score was brought into consideration as a representative factor for predicting immune escape and immune dysfunction, both of which are factors that determine the efficacy of immunotherapy [22,23]. In our study, the IRPS high-risk group was associated with significantly higher TIDE score (P < 0.001, Fig. 14). These findings support the idea that IRPS high-risk patients may fail to benefit from immunotherapy.

To evaluate IRPS-associated outcomes in a realistic scenario, we obtained clinical and molecular data from a ccRCC cohort treated with anti-PD-1 therapy [19] as an external validation data set. A total of 309 ccRCC patients with suitable RNA-seq expression and clinical data were included. The efficacy of anti-PD-1 therapy within IRPS risk group was explored. We calculated the IRPS risk score for each patient in Braun et al.'s cohort, and the progression free survival (PFS) and overall survival (OS) after anti-PD-1 therapy were explored. Furthermore, multivariate Cox proportional hazards regression analysis was deployed to test the independent predictive ability of IRPS. According to the multivariate Cox proportional hazards regression analysis, The IRPS risk score was an independent signature and had prominent association with PFS and OS. Patients in the IRPS low risk group had better PFS (HR:0.73; 95% CI: 0.54–1.0; P = 0.047, Fig. 15A) and higher IRPS risk score was associated with worse OS (HR:1.5; 95% CI: 1.01–2.3; P = 0.047, Fig. 15B).

Furthermore, subgroup analysis showed that IRPS was a predictor of PFS. Patients with IRPS low risk in the female subgroup (HR:0.52; 95% CI:0.30–0.92; P = 0.0245) and the younger subgroup (age≤65 years old, HR:0.67; 95% CI:0.45–0.98; P = 0.037) were likely to have a better outcome (Fig. 16). This finding suggests that IRPS risk score may be more predictive in younger or female patients.

To further validate the predictive value of IRPS in ICI treatment, the Cancer Immunome Atlas (TCIA) database was utilized for downloading the immunophenoscore (IPS) of ccRCC patients. Several studies [24–27] have reported the role of IPS in predicting the immunotherapy response. Patients with high IPS generally respond well to ICI treatment. The relationship between IPS and IRPS risk group was analyzed as a surrogate for the likely response to ICI treatment. We found that the IPS was significantly different within IRPS risk groups, and patients in IRPS low-risk group presented with higher IPS (P < 0.001, Fig. 17). Accordingly, IRPS is likely to predict the efficacy of immune checkpoint inhibitors.
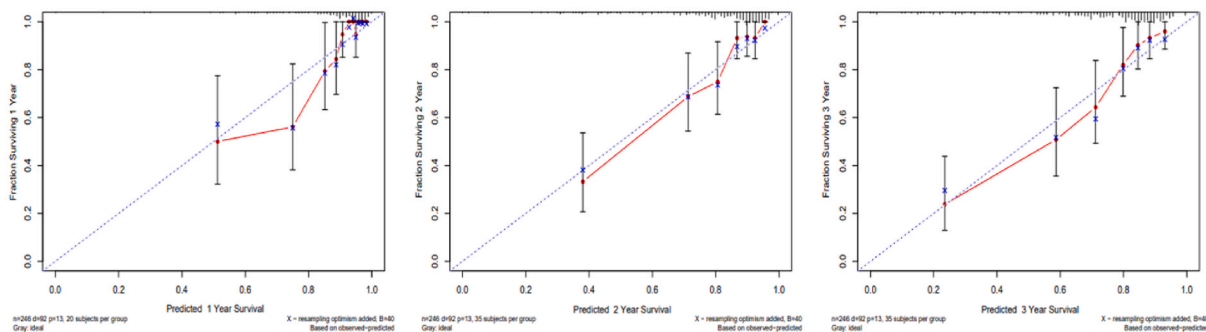
A
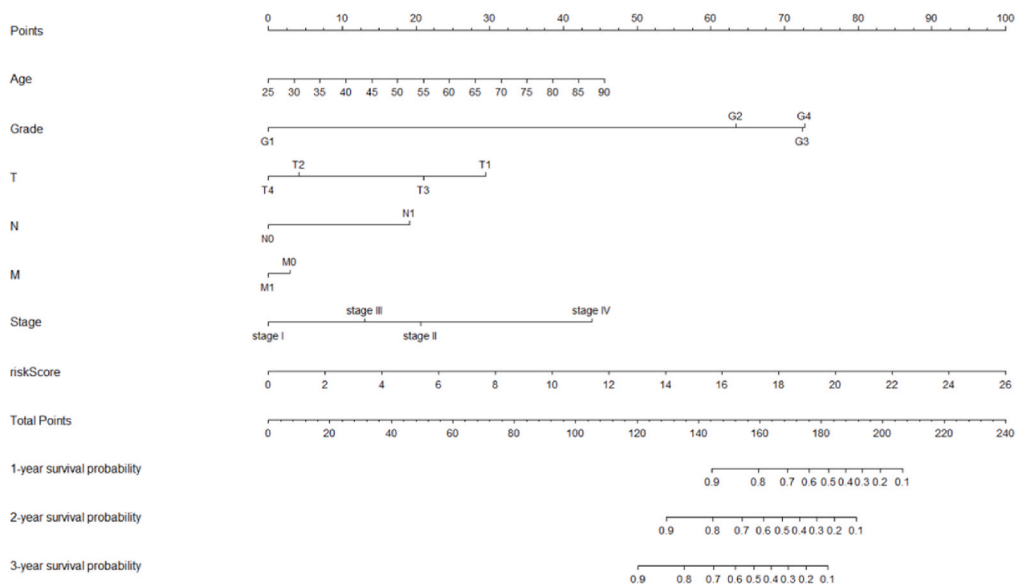
B

Fig. 9. Construction and Validation of the prognostic nomogram. (A) The 1-/2-/3-year survival prognostic nomogram including IRPS risk score and other clinical factors. (B) The calibration curves of the nomogram prediction of the 1-/2-/3-year OS of ccRCC patients. The blue dotted line represents the perfect prediction of the nomogram.

In order to explore the performance of IRPS in a cohort of metastatic ccRCC, 84 metastatic ccRCC patients with available RNA-seq expression and clinical data were obtained from Braun et al.'s ccRCC cohort [19]. As shown, IRPS high-risk was associated with high expression of PD-L1 in metastatic ccRCC (Fig. S2).

Finally, we used ROC curve and AUC to present the prognostic value of the IRPS model. The 1-year survival AUC of the ROC curve was 0.814, 2-year survival AUC of the ROC curve was 0.756, and 3-year survival AUC of the ROC curve was 0.773, implying that IRPS were highly precise for forecasting survival outcomes (Fig. 18A). Moreover, in order to claim the predictive value of IRPS, we compared IRPS with other published gene signatures. An 18 gene signature developed by Li et al. [18] strongly related to clinical prognosis. We found that IRPS had better predictive value (Fig. 18B), with the 3-year survival AUC of 0.773.

4. Discussion

Improving low survival rates in advanced and metastatic ccRCC is a continuing focus of clinical research and development [28]. Immune checkpoint inhibition (ICI) treatment has improved prognosis and represents the most effective new strategy in ccRCC [29]. Nevertheless, not every patient can benefit from immunotherapy due to immune dysfunction and exclusion. In order to provide more
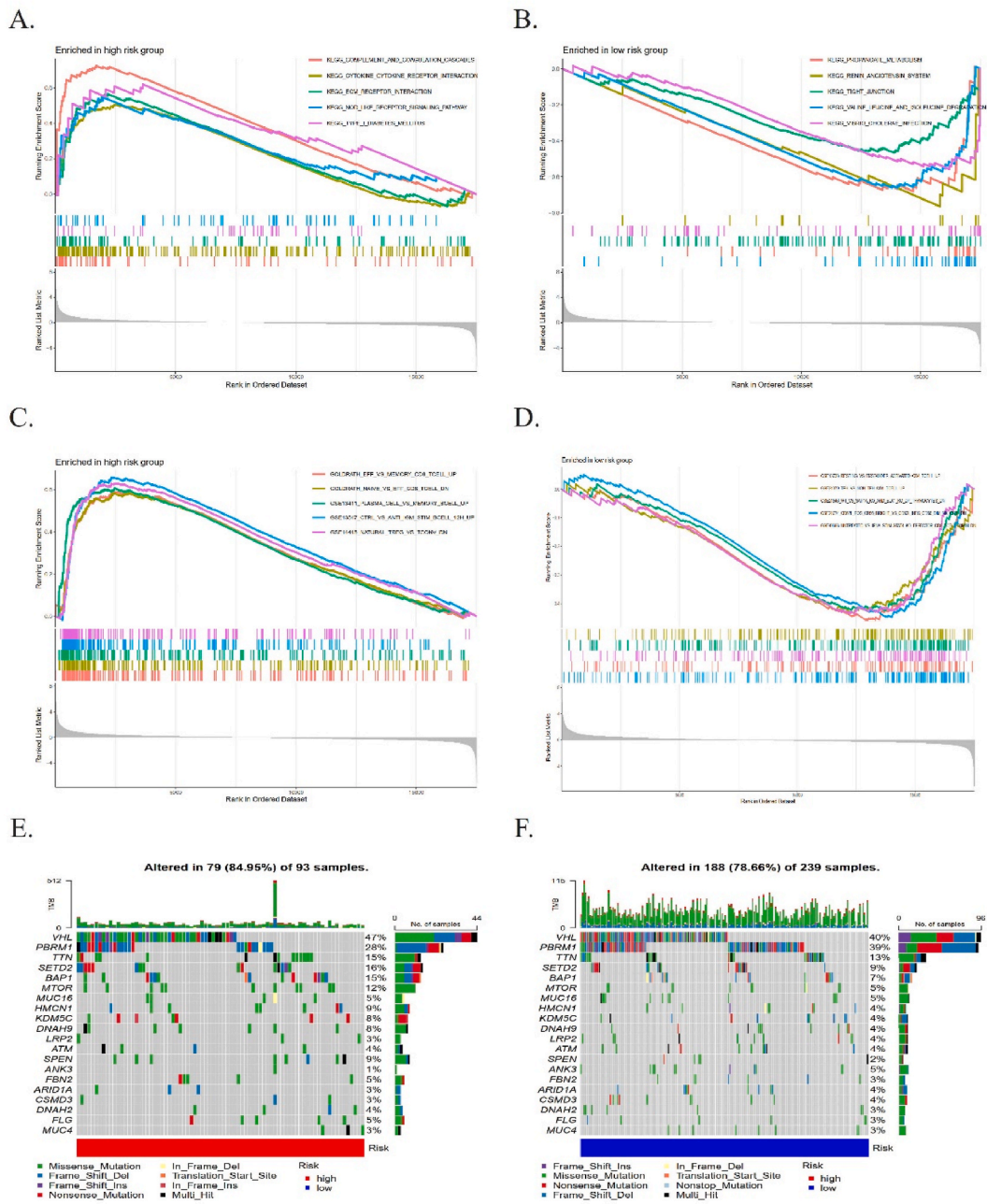
Fig. 10. Molecular characteristics and immunologic mechanisms are significantly different within IRPS risk subgroups. (A) GSEA analysis showing that complement and coagulation cascades, cytokine-cytokine receptor interaction, ECM receptor interaction, NOD link receptor signaling pathway and type I diabetes mellitus are significantly enriched in the IRPS high risk subgroup. (B) GSEA analysis showing that propanoate metabolism, renin angiotensin system, tight junction, valine leucine and isoleucine degradation, vibrio cholerae infection are enriched in the IRPS low risk subgroup. (C) GSEA analysis showing that B cells and natural T reg cells are enriched in the IRPS high risk subgroup. (D) GSEA analysis showing that CD4 T cells, CD4 follicular helper T cells, NK cells and CD8 T cells are enriched in the IRPS low risk subgroup. (E), (F) Waterfall plot of significantly different mutated genes within the high risk and low risk IRPS subgroups.

individualized prognoses and tailored therapy for ccRCC patients, it is crucial to explore reliable signatures for forecasting the effectiveness of ICI treatment. Recently, immune-related genes seemed to have prognostic ability in ccRCC [30–32]. However, previous projects only focused on OS or the potential mechanism in tumor immune microenvironment and failed to explore the relationship between immune-related biomarkers and the efficacy of immunotherapy.

In current project, we established a IRPS for ccRCC and split patients into two groups according to risk score by applying an optimal cut-off point. Compared with the low-risk group, we found that high risk people presented to be elder (62.4 ± 12.3 years old, P =
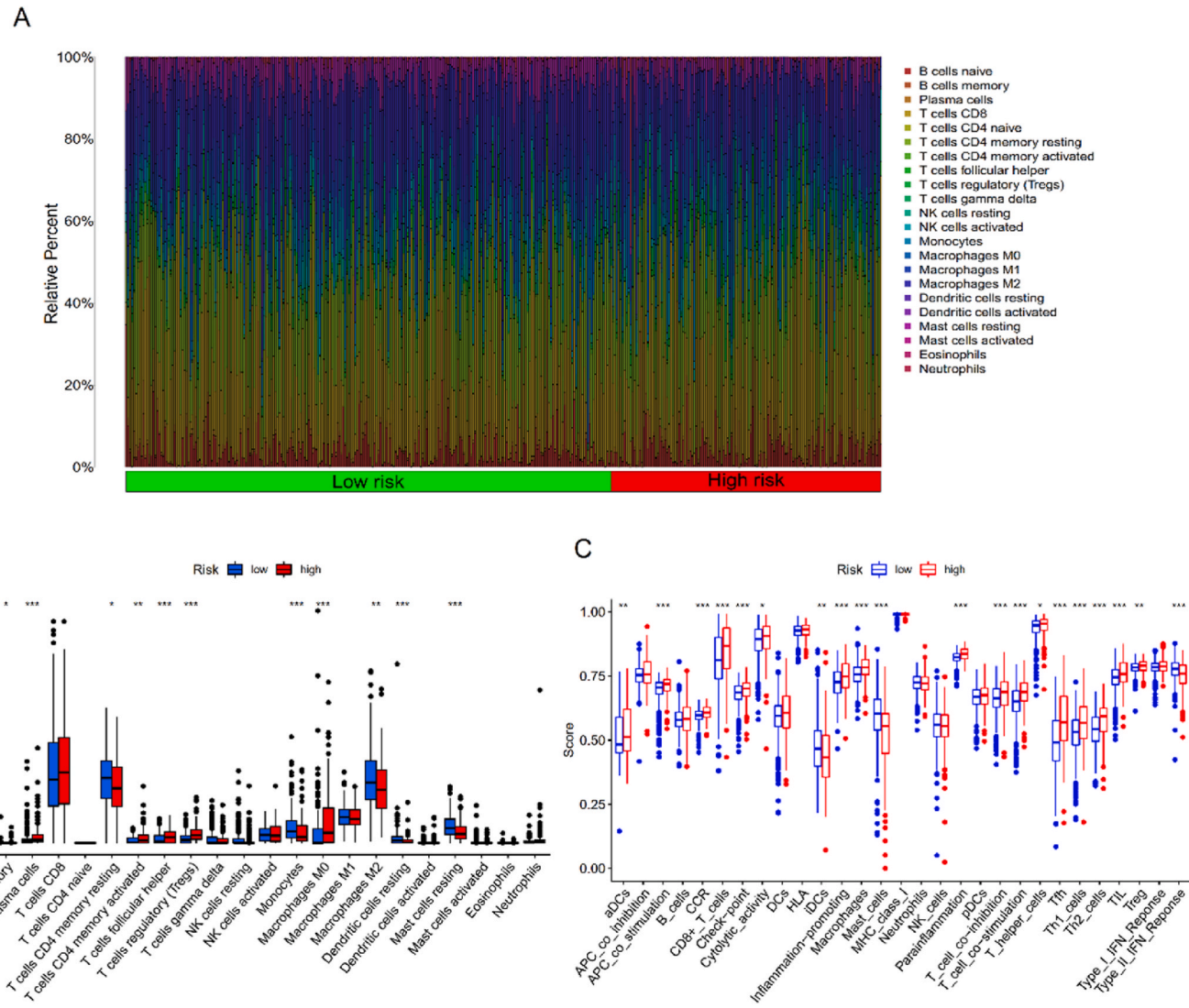
Fig. 11. Immune characteristics of different IRPS subgroups. (A) The bar plot of the proportions of the 22 immune cell subtypes in the TCGA cohort. (B) The violin plot of the 22 immune cell subtypes in high risk and low risk IRPS subgroup. (C) ssSGEA analysis of Immune functions in different IRPS subgroups.
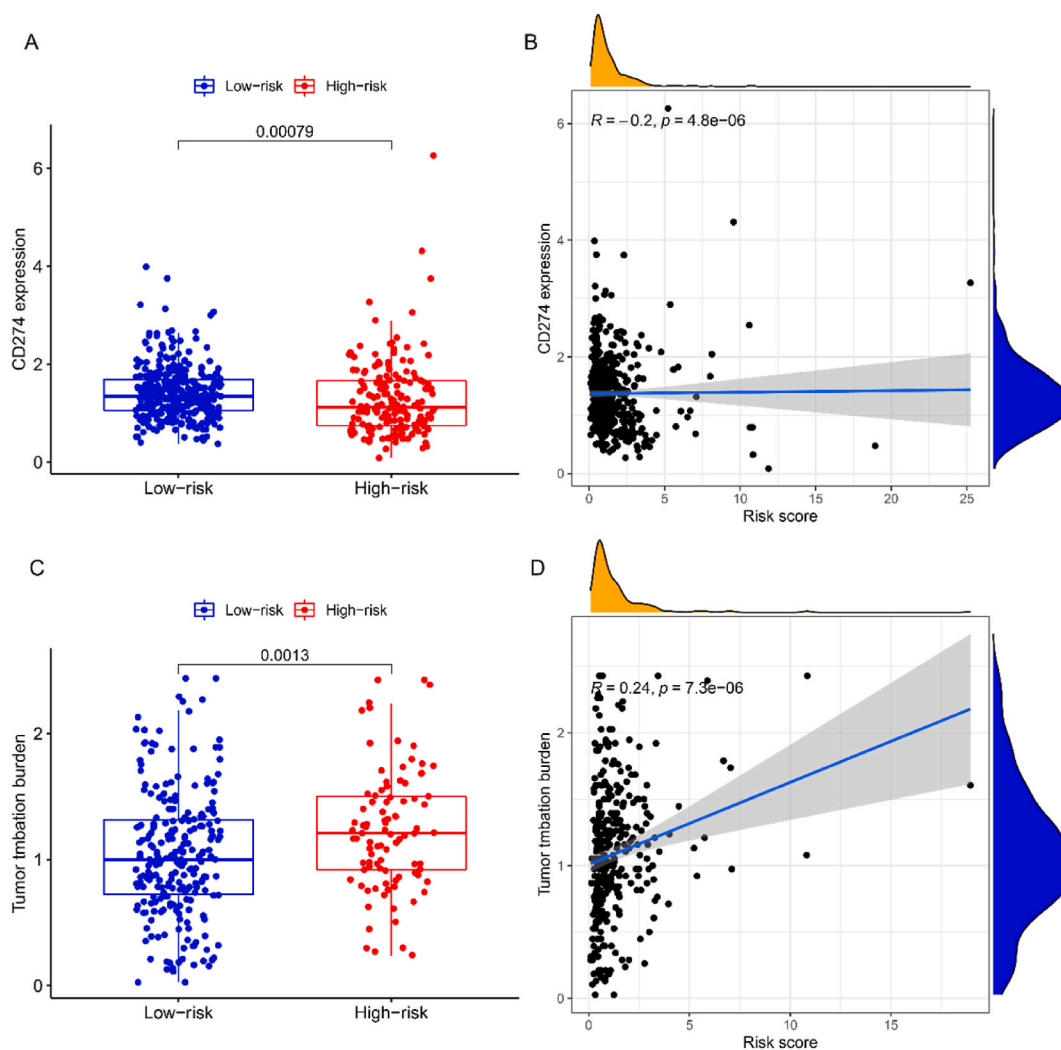
Fig. 12. Correlation between IRPS and PD-L1 expression and TMB. (A) The IRPS low-risk ccRCCs have higher PD-L1 expression (P < 0.001). (B) IRPS risk score negatively correlates with PD-L1 expression (R = −0.2, P < 0.001). (C) The IRPS low-risk ccRCCs have lower TMB (P = 0.0013). (D) IRPS risk score positively associates with TMB (R = 0.24, P < 0.001.

0.015), diagnose with advanced tumor stage (stage III-IV, 62.7%) and advanced grade (grade III-IV, 77.5%), and poorer survival (p < 0.001). Furthermore, multivariate analysis demonstrated that IRPS was an isolated biomarker related to survival in ccRCC.

The IRPS we identified is characterized by 10 immune-related genes, including TMSB4Y, NDRG1, SEMA3G, SEMA6D, BMP1, TSLP, MCHR1, SHC1, PRKX, TRIM55. According to the coefficient of each gene, we determined that patients with low expression of TMSB4Y, NDRG1, SEMA3G, SEMA6D, PRKX and TRIM55, as well as high expression of BMP1, TSLP, MCHR1 and SHC1 may have high risk of immune dysfunction and exclusion. According to previous research, TMSB4Y has tumor suppressor properties, as a gene encoding the actin sequestering protein [33]. Laryngeal cancer patients with low TMSB4Y expression have been proved to have poor outcomes [34]. N-Myc Downstream-Regulated Gene 1 (NDRG1) is one of the NDRG family of proteins, and is considered to possess anti-oncogenic and anti-metastatic effects in many cancers [35], but has also been suggested to have a pro-tumorigenesis function in kidney [36]. SEMA3G is one of the members of the Class-3 semaphorins (SEMA3), and plays a tumor inhibiting role in kidney cancer [37]. High expression of SEMA6D in breast cancer has close relationship with better survival outcomes [38]. The human protein kinase X gene (PRKX) induces apoptosis and causes Sunitinib resistance in kidney carcinoma [39]. TRIM55 over-expression suppresses tumor migration and invasion in lung adenocarcinoma [40]. BMP1 over-expression leads to tumor progression and reflects poor survival outcomes in ccRCC [41]. TSLP and SHC1 are reported to have a considerable role in induction and progression of cancer [42,43]. All these reports are consistent with our IRPS biomarker signature.

CIBERSORT results comparing IRPS risk subgroups, suggested that the high-risk group contained significantly more T cells regulatory (Tregs) than the low-risk group. Treg cells, a specific subpopulation of T cells, perform the function of inhibiting the immune response. Tregs maintain the crucial balance of immune microenvironment by inhibiting the proliferation of T cells. However, some
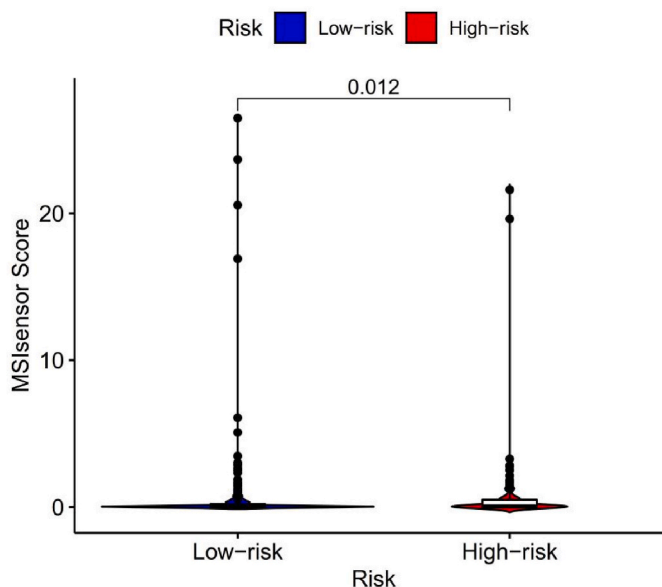
Fig. 13. The relationship between MSIsensor score and IRPS subgroups. Comparison of the MSIsensor score between patients in different IRPS risk groups reveal that the IRPS high-risk group has a higher average MSIsensor score (P = 0.012).
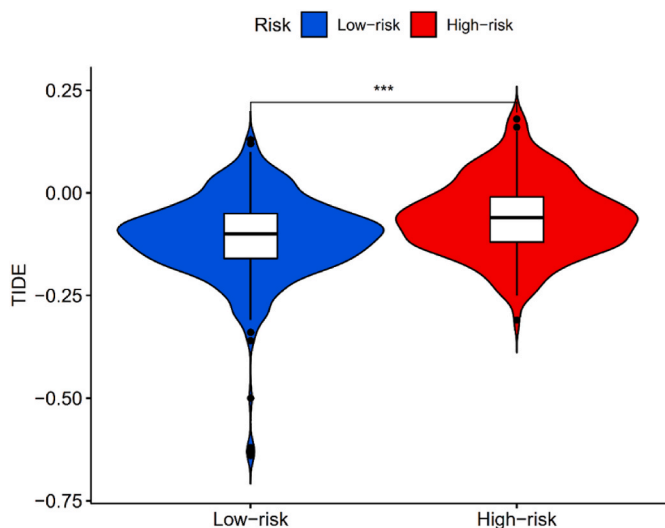

Fig. 14. Tumor immune dysfunction and exclusion (TIDE) score in different IRPS subgroups. Comparison of the TIDE score between patients in different IRPS risk groups reveal that the IRPS high-risk group has a higher average TIDE score (P < 0.001).

studies suggests that excessive enrichment of Tregs can accelerate tumor progression and induce immune dysfunction and exclusion [44,45]. Therefore, we speculate that as the result of the abundance of Tregs, patients in IRPS high-risk group have poor outcomes and failed to response for the immunotherapy.

For instance, PD-L1 expression may fail to predict benefit from ICI treatment due to the following reasons: 1) heterogeneity of PD-L1 expression; 2) Various factors in the internal environment simultaneously influencing PD-L1 expression; 3) driver mutations affecting PD-L1 expression [12,14,46]. Similarly, patients with high TMB are expected to benefit from ICI therapy, but the literature demonstrates this is not always the case [47]. Importantly, the selection of tissue specimens affects the detection of TMB and single-site biopsy might overestimate the level of clonal mutation [14]. However, although there are multiple challenges with using PD-L1 expression or TMB as biomarkers, they are still the best predictors of ICI treatment effect currently. Therefore, we used these important, but imperfect measures as a tool to give us some notion of the likely ICI responsiveness of IRPS low-risk and high-risk tumors.

According to our study, patients in the IRPS high-risk group were have low PD-L1 expression and high TMB. As previously reported [12], patients with high TMB often respond adequately to ICI therapy. On the contrary, patients in IRPS high-risk group who we predict
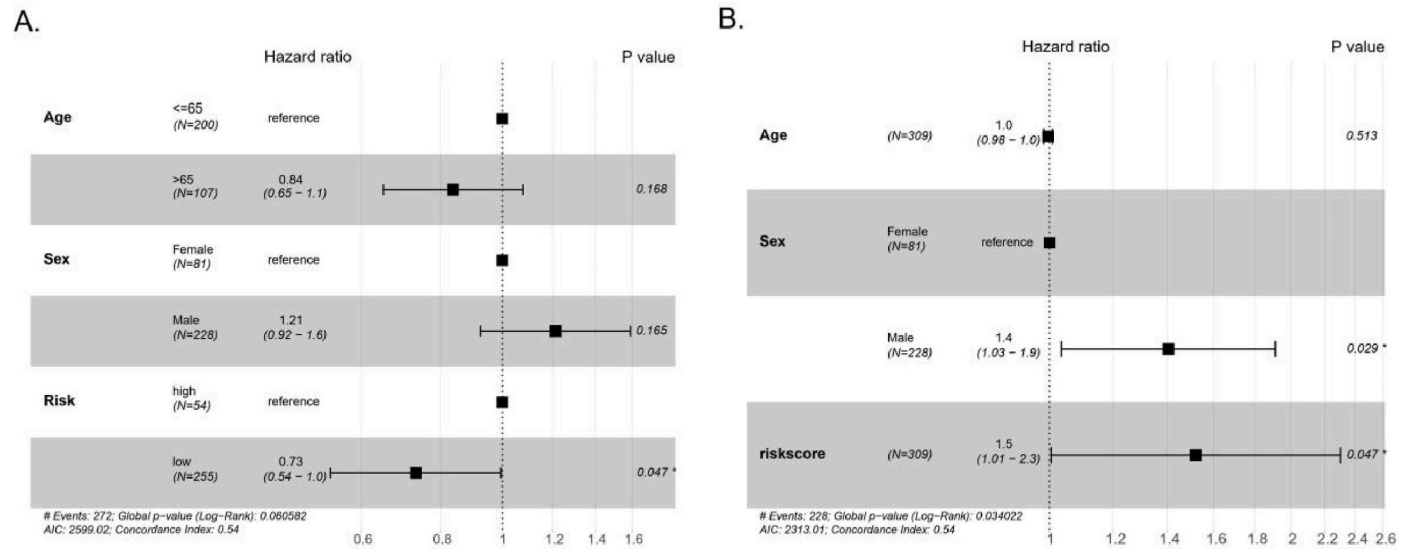
Fig. 15. Multivariate Cox regression analysis reveal the IRPS risk score is an independent prognostic factor in a cohort of ICI-treated ccRCC patients. (A) Multivariate Cox regression analysis demonstrates that patients in the IRPS low risk group have better PFS (HR:0.73; 95%CI: 0.54–1.0; P = 0.047). (B) Multivariate Cox regression analysis demonstrates that higher IRPS risk score is associated with worse OS (HR:1.5; 95%CI: 1.01–2.3; P = 0.047).
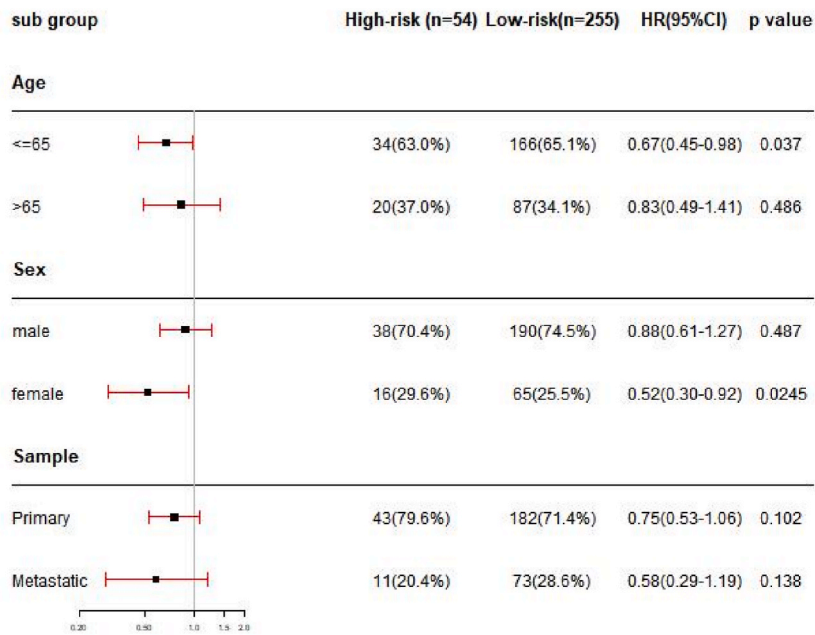
sub group	High-risk (n=54)	Low-risk(n=255)	HR(95%CI)	p value
Age				
<=65	34(63.0%)	166(65.1%)	0.67(0.45-0.98)	0.037
>65	20(37.0%)	87(34.1%)	0.83(0.49-1.41)	0.486
Sex				
male	38(70.4%)	190(74.5%)	0.88(0.61-1.27)	0.487
female	16(29.6%)	65(25.5%)	0.52(0.30-0.92)	0.0245
Sample				
Primary	43(79.6%)	182(71.4%)	0.75(0.53-1.06)	0.102
Metastatic	11(20.4%)	73(28.6%)	0.58(0.29-1.19)	0.138

Fig. 16. Subgroup analysis of the ICI treatment cohort demonstrating that IRPS is a predictor of PFS. In the female subgroup (HR:0.52; 95% CI:0.30–0.92; P = 0.0245) and the younger subgroup (age≤65 years old, HR:0.67; 95% CI:0.45–0.98; P = 0.037), patients with IRPS low risk are likely to have a better outcome.
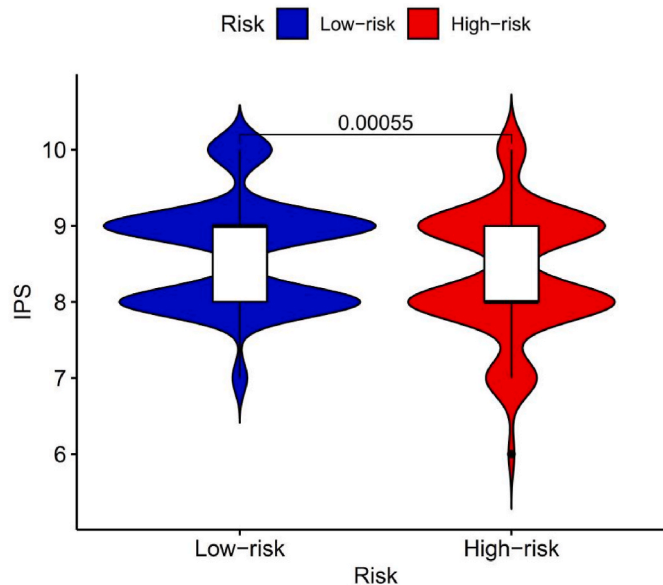

Fig. 17. Comparison of Immunophenoscore in IRPS Risk Groups. Comparison of IPS between the IRPS risk groups revealing that IRPS high-risk ccRCCs have a reduced average immunophenoscore (P < 0.001).

may fail to benefit from immunotherapy, may have high TMB. Though seemingly paradoxical, our findings could be explained by the following facts: 1) TMB varies in different cancer types. Compared with other cancer types, the TMB of ccRCC patients is not significant [48]. Therefore, TMB might not be a perfect marker to predict the prognosis in ccRCC patients [49]. 2) The predictive value of TMB for ICI therapy in ccRCC is still controversial. Although several clinical trials demonstrate a correlation between high TMB and immunotherapy efficacy [50,51], some studies suggest that ccRCC has unique features in terms of the immune microenvironment and ccRCC patients with high TMB have a lower reaction rate to immunotherapy [15,16,52,53]. In this way, ccRCC patients in the IRPS high-risk group with high TMB may potentially fail to respond to immunotherapy. 3) Due to the lack of large clinical samples to further verify the
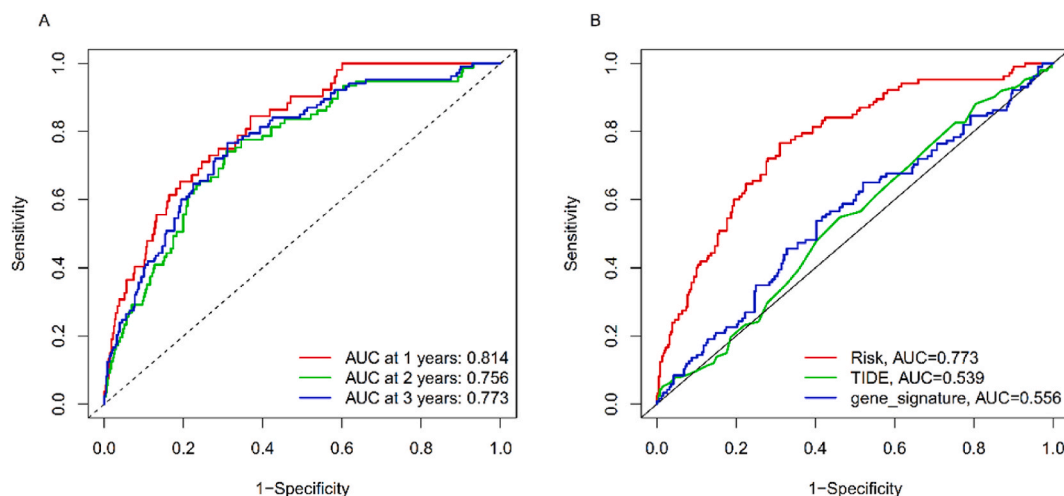
Fig. 18. (A) The prediction of IRPS for prognosis at one, three and five years in the entire TCGA cohort. (B) ROC analysis of IRPS, 18-gene signature, and TIDE on overall survival in the entire TCGA cohort.

prognostic effect of TMB, our study still has some limitations. Relevant big sample clinical trials are needed in the future. Therefore, it is plausible that ccRCC patients in the IRPS high-risk group with high TMB may potentially fail to respond to immunotherapy, and the combination of these two biomarkers and others may allow for improved personalized treatment.

Tumor Immune Dysfunction and Exclusion (TIDE) is a signature to quantify the dysfunction of T cells and immune exclusion in order to predict the immune reaction [54]. TIDE includes the effect of the cellular immune reaction in tumor infiltrating cytotoxic T lymphocytes (CTL) dysfunction and immune exclusion of CTL by immunosuppressive factors. Several studies hint that patients who were diagnosed with high TIDE score might perform more immune escape and immune dysfunction, indicating lower reaction to immunotherapy [55]. TIDE score had spectacular success in predicting immune reaction of patient treated with immunotherapy in many cancers [56,57]. Consequently, we used TIDE in our study to assess the predictive value of IRPS for immune dysfunction and exclusion. The high-risk IRPS group had high TIDE score, which implied patients in the high-risk group might experience immune escape and no response to immunotherapy. Nevertheless, TIDE focused only on predicting the response to immunotherapy in patients with ccRCC, rather than OS. We found that IRPS presented to be a better biomarker to both predict the efficacy of ICIs and OS in ccRCC patients.

A nomogram was built to visualize the prediction model for 1-year, 2-year and 3-year probabilities of mortality in patients with ccRCC. The 1-/2-/3-year survival AUC of our model was greater than 0.7, implying that IRPS significant predictive value for OS. Comparison among TIDE score and another gene signature [18] performed that IRPS was a better predictor of OS.

The findings of our research could be useful to clinicians in providing a novel immune response prediction signature for the efficacy of immunotherapy in ccRCC patients. However, there are still some limitations in our study. First of all, this novel prognostic model was established based on the public RNA-seq expression data from TCGA database, and validated by one external data set from GEO data base, thereby leading to potential selection bias. Therefore, further researches are needed to enlarge the sample volume. Next, although the predictive ability of IRPS was compared with other gene signatures using TCGA and successfully performed as to be an independent factor of OS and the efficacy of immunotherapy, this 10-gene signature will need to be further analyzed in real world study. Finally, further laboratory experiments and study on mechanism are imminently needed to reveal the function of IRPS genes in ccRCC.

5. Conclusion

In general, this research established and validated a 10 -gene immune-related signature which was predictive of the efficacy of immunotherapy and overall survival in ccRCC. These results may provide a novel independent biomarker to identify potential ccRCC patients with good immune response. Furthermore they may be helpful to individualize treatment.

Author contribution statement

Jiannan Yao: Conceived and designed the experiments; Wrote the paper.
Ziwei Liang: Performed the experiments; Analyzed and interpreted the data; Wrote the paper.
Ling Duan: Analyzed and interpreted the data.
Yang Ge; Jian Liu; Guangyu An: Contributed reagents, materials, analysis tools or data.

Data availability statement

The datasets utilized to claim the findings of our research are publicly available from the TCGA database (https://portal.gdc. cancer.gov/), GEO database, GSE22541 (https://www.ncbi.nlm.nih.gov/geo/), ImmPort (https://www.immport.org/shared/ home), InnateDB (https://www.innateDBdb.com/) databases and TIDE (http://tide.dfci.harvard.edu/).

Declaration of competing interest

The authors declare that they have no known competing financial interests or personal relationships that could have appeared to influence the work reported in this paper

Abbreviations

RCC	Renal cell carcinoma
ccRCC	Clear cell renal cell carcinoma
IRPS	Immune response prediction signature
TCGA	The Cancer Genome Atlas
GEO	Gene Expression Omnibus
TIDE	Tumor immune dysfunction and exclusion
ICI	Immune checkpoint inhibitor
DEGs	differentially expressed genes
IRDEGs	Immune-related differentially expressed genes
WGCNA	Weighted Gene Co-expression Network Analysis
LASSO	Least Absolute Shrinkage and Selection Operator method
TIDE	Tumor immune dysfunction and exclusion
FDA	Food and Drug Administration
TMB	Tumor Mutational Burden
FDR	False Discovery Rate
GO	Gene Ontology
KEGG	Kyoto Encyclopedia of Genes and Genomes
TOM	topological overlap measure
OS	overall survival
GSEA	Gene set enrichment analysis
ROC	receiver operator characteristic
AUC	area under the curve

Appendix A. Supplementary data

Supplementary data to this article can be found online at https://doi.org/10.1016/j.heliyon.2023.e15925.

References

[1] R.L. Siegel, et al., Cancer statistics, 2022, CA Cancer J. Clin. 72 (1) (2022) 7–33.
[2] L. Vuong, et al., Tumor microenvironment dynamics in clear-cell renal cell carcinoma, Cancer Discov. 9 (10) (2019) 1349–1357.
[3] S. Negrier, et al., Randomized study of intravenous versus subcutaneous interleukin-2, and IFNalpha in patients with good prognosis metastatic renal cancer, Clin. Cancer Res. 14 (18) (2008) 5907–5912.
[4] S.A. Padala, et al., Epidemiology of renal cell carcinoma, World J. Oncol. 11 (3) (2020) 79–87.
[5] R.J. Motzer, et al., Nivolumab versus everolimus in advanced renal-cell carcinoma, N. Engl. J. Med. 373 (19) (2015) 1803–1813.
[6] D.F. Mcdermott, et al., Open-Label, single-arm, phase II study of pembrolizumab monotherapy as first-line therapy in patients with advanced non–clear cell renal cell carcinoma, J. Clin. Oncol. 39 (9) (2021). JCO.20.02365.
[7] T. Powles, et al., Pembrolizumab plus axitinib versus sunitinib monotherapy as first-line treatment of advanced renal cell carcinoma (KEYNOTE-426): extended follow-up from a randomised, open-label, phase 3 trial, Lancet Oncol. 21 (12) (2020) 1563–1573.
[8] J. Zhang, et al., Targeting WD repeat domain 5 enhances chemosensitivity and inhibits proliferation and programmed death-ligand 1 expression in bladder cancer, J. Exp. Clin. Cancer Res. 40 (1) (2021) 203.
[9] M. Huang, et al., HSF1 facilitates the multistep process of lymphatic metastasis in bladder cancer via a novel PRMT5-WDR5-dependent transcriptional program, Cancer Commun. (Lond) 42 (5) (2022) 447–470.
[10] Q.H. Zhou, et al., HHLA2 and PD-L1 co-expression predicts poor prognosis in patients with clear cell renal cell carcinoma, J. Immunother. Cancer 8 (1) (2020).
[11] E.B. Garon, et al., Pembrolizumab for the treatment of non-small-cell lung cancer, N. Engl. J. Med. 372 (21) (2015) 2018–2028.
[12] P.A. Ott, et al., T-Cell–Inflamed gene-expression profile, programmed death ligand 1 expression, and tumor mutational burden predict efficacy in patients treated with pembrolizumab across 20 cancers: keynote-028, J. Clin. Oncol. 37 (4) (2019) 318–327.
[13] D.T. Le, et al., Mismatch repair deficiency predicts response of solid tumors to PD-1 blockade, Science 357 (6349) (2017) 409–413.
[14] M. Yi, et al., Biomarkers for predicting efficacy of PD-1/PD-L1 inhibitors, Mol. Cancer 17 (1) (2018) 129.

[15] A. Simonaggio, et al., Tumor microenvironment features as predictive biomarkers of response to immune checkpoint inhibitors (ICI) in metastatic clear cell renal cell carcinoma (mccRCC), Cancers (2) (2021).

[16] D.J. McGrail, et al., High tumor mutation burden fails to predict immune checkpoint blockade response across all cancer types, Ann. Oncol. 32 (5) (2021) 661–672.

[17] P. Langfelder, S. Horvath, WGCNA: an R package for weighted correlation network analysis, BMC Bioinf. 9 (2008) 559.

[18] G. Li, et al., Identification of an independent immune-genes prognostic index for renal cell carcinoma, BMC Cancer 21 (1) (2021) 746.

[19] D.A. Braun, et al., Interplay of somatic alterations and immune infiltration modulates response to PD-1 blockade in advanced clear cell renal cell carcinoma, Nat. Med. 26 (6) (2020) 909–918.

[20] K. Ganesh, et al., Immunotherapy in colorectal cancer: rationale, challenges and potential, Nat. Rev. Gastroenterol. Hepatol. 16 (6) (2019) 361–375.

[21] B. Niu, et al., MSIsensor: microsatellite instability detection using paired tumor-normal sequence data, Bioinformatics 30 (7) (2014) 1015–1016.

[22] T.G. Shrihari, Innate and adaptive immune cells in Tumor microenvironment, Gulf J. Oncol. 1 (35) (2021) 77–81.

[23] Joyce, et al., T cell exclusion, immune privilege, and the tumor microenvironment, Science (2015).

[24] P. Charoentong, et al., Pan-cancer immunogenomic analyses reveal genotype-immunophenotype relationships and predictors of response to checkpoint blockade, Cell Rep. 18 (1) (2017) 248–262.

[25] J.N. Guo, et al., Identification and quantification of immune infiltration landscape on therapy and prognosis in left- and right-sided colon cancer, Cancer Immunol. Immunother. 71 (6) (2022) 1313–1330.

[26] J. Wu, et al., A risk model developed based on tumor microenvironment predicts overall survival and associates with tumor immunity of patients with lung adenocarcinoma, Oncogene 40 (26) (2021) 4413–4424.

[27] M. Yi, et al., Immune signature-based risk stratification and prediction of immune checkpoint inhibitor's efficacy for lung adenocarcinoma, Cancer Immunol. Immunother. 70 (6) (2021) 1705–1719.

[28] S. Chevrier, et al., An immune Atlas of clear cell renal cell carcinoma, Cell 169 (4) (2017) 736–749 e18.

[29] W. Xu, M.B. Atkins, D.F. McDermott, Checkpoint inhibitor immunotherapy in kidney cancer, Nat. Rev. Urol. 17 (3) (2020) 137–150.

[30] Y. Zou, C. Hu, A 14 immune-related gene signature predicts clinical outcomes of kidney renal clear cell carcinoma, PeerJ 8 (2020), e10183.

[31] Z. Tao, et al., A united risk model of 11 immune related gene pairs and clinical stage for prediction of overall survival in clear cell renal cell carcinoma patients, Bioengineered 12 (1) (2021) 4259–4277.

[32] B. Wan, et al., Prognostic value of immune-related genes in clear cell renal cell carcinoma, Aging (Albany NY) 11 (23) (2019).

[33] H.Y. Wong, et al., TMSB4Y is a candidate tumor suppressor on the Y chromosome and is deleted in male breast cancer, Oncotarget 6 (42) (2015).

[34] B. Lu, et al., miR-183/TMSB4Y, a new potential signaling axis, involving in the progression of laryngeal cancer via modulating cell adhesion, J. Recept. Signal Transduct. Res. (1) (2020) 1–8.

[35] J. Chekmarev, M.G. Azad, D.R. Richardson, The oncogenic signaling disruptor, NDRG1: molecular and cellular mechanisms of activity, Cells 10 (9) (2021).

[36] B.A. Fang, et al., Molecular functions of the iron-regulated metastasis suppressor, NDRG1, and its potential as a molecular target for cancer therapy, BBA - Rev. Cancer 1845 (1) (2014) 1–19.

[37] X. Zhang, et al., A pan-cancer study of class-3 semaphorins as therapeutic targets in cancer, BMC Med. Genom. 13 (Suppl 5) (2020) 45.

[38] T.A. Hughes, MiR-195 and its target SEMA6D regulate chemoresponse in breast cancer, Cancers 13 (2021).

[39] C. Bender, A. Ullrich, PRKX, TTBK2 and RSK4 expression causes Sunitinib resistance in kidney carcinoma- and melanoma-cell lines, Int. J. Cancer 131 (2) (2012) E45–E55.

[40] T. Guo, et al., TRIM55 suppresses malignant biological behavior of lung adenocarcinoma cells by increasing protein degradation of Snail1, Cancer Biol. Ther. 23 (1) (2022) 17–26.

[41] W. Xiao, et al., Overexpression of BMP1 reflects poor prognosis in clear cell renal cell carcinoma, Cancer Gene Ther. 27 (5) (2020) 330–340.

[42] J. Corren, S.F. Ziegler, TSLP: from allergy to cancer, Nat. Immunol. 20 (12) (2019) 1603–1609.

[43] K.D. Wright, et al., The p52 isoform of SHC1 is a key driver of breast cancer initiation, Breast Cancer Res. 21 (1) (2019) 74.

[44] S. Dees, et al., Regulatory T cell targeting in cancer: emerging strategies in immunotherapy, Eur. J. Immunol. 51 (2) (2021) 280–291.

[45] V. Sasidharan Nair, E. Elkord, Immune checkpoint inhibitors in cancer therapy: a focus on T-regulatory cells, Immunol. Cell Biol. 96 (1) (2018) 21–33.

[46] A.J. Schoenfeld, et al., Clinical and molecular correlates of PD-L1 expression in patients with lung adenocarcinomas, Ann. Oncol. 31 (5) (2020) 599–608.

[47] D.J. Mcgrail, et al., High tumor mutation burden fails to predict immune checkpoint blockade response across all cancer types, Ann. Oncol. (2021).

[48] L.B. Alexandrov, et al., Signatures of mutational processes in human cancer, Nature 500 (7463) (2013) 415–421.

[49] R.M. Samstein, et al., Tumor mutational load predicts survival after immunotherapy across multiple cancer types, Nat. Genet. 51 (2) (2019) 202–206.

[50] A. Marabelle, et al., Association of tumour mutational burden with outcomes in patients with advanced solid tumours treated with pembrolizumab: prospective biomarker analysis of the multicohort, open-label, phase 2 KEYNOTE-158 study, Lancet Oncol. 21 (10) (2020) 1353–1365.

[51] M.D. Hellmann, et al., Genomic features of response to combination immunotherapy in patients with advanced non-small-cell lung cancer, Cancer Cell 33 (5) (2018) 843–852 e4.

[52] C. Zhang, et al., Exploration of the relationships between tumor mutation burden with immune infiltrates in clear cell renal cell carcinoma, Ann. Transl. Med. 7 (22) (2019) 648.

[53] S. Xu, et al., Cuproptosis-associated lncRNA establishes new prognostic profile and predicts immunotherapy response in clear cell renal cell carcinoma, Front. Genet. 13 (2022), 938259.

[54] P. Jiang, et al., Signatures of T cell dysfunction and exclusion predict cancer immunotherapy response, Nat. Med. 24 (10) (2018) 1550–1558.

[55] Q. Wang, et al., Analysis of immune-related signatures of lung adenocarcinoma identified two distinct subtypes: implications for immune checkpoint blockade therapy, Aging 12 (4) (2020) 3312–3339.

[56] C. Ding, et al., Characterization of the fatty acid metabolism in colorectal cancer to guide clinical therapy, Mol. The.r Oncolytics 20 (2021) 532–544.

[57] W. Zhong, et al., Characterization of molecular heterogeneity associated with tumor microenvironment in clear cell renal cell carcinoma to aid immunotherapy, Front. Cell Dev. Biol. 9 (2021), 736540.